Published in final edited form as:
Magn Reson Imaging. 2011 November ; 29(9): 1165–1174. doi:10.1016/j.mri.2011.07.012.

Alterations in diffusion properties of white matter in Williams syndrome

Lori R. Arlinghaus[1,2], **Tricia A. Thornton-Wells**[1,3,4], **Elisabeth M. Dykens**[3,5], and **Adam W. Anderson**[1,2,6]

[1]Institute of Imaging Science, Vanderbilt University, Nashville, Tennessee

[2]Department of Radiology and Radiological Sciences, Vanderbilt University, Nashville, Tennessee

[3]Vanderbilt University Kennedy Center for Research on Human Development, Vanderbilt University, Nashville, Tennessee

[4]Department of Molecular Physiology & Biophysics, Center for Human Genetics Research, Vanderbilt University, Nashville, Tennessee

[5]Department of Psychology & Human Development, Vanderbilt University, Nashville, Tennessee

[6]Department of Biomedical Engineering, Vanderbilt University, Nashville, Tennessee

Abstract

Diffusion tensor imaging (DTI) was used to investigate the involvement of brain white matter in Williams syndrome (WS), a genetic neurodevelopmental disorder. Whole-brain DTIs were obtained from 16 young adults with WS and 16 normal controls. A voxel-based analysis was performed to compare fractional anisotropy (FA) values between the two groups. A tract-based analysis was also performed to compare FA values between the two groups along two major white matter tracts that pass through the external capsule: the uncinate and inferior fronto-occipital fasciculi. Several regions of both increased and decreased FA were found within major white matter tracts that connect functional regions that have previously been implicated in the cognitive and neurological symptoms of the syndrome. The tract-based analysis provided additional insight into the involvement of specific white matter tracts implicated in the voxel-based analysis within the external capsule. The results from this study support previously reported changes in white matter diffusion properties in WS and demonstrate the potential usefulness for tract-based analysis in future studies of the disorder.

Keywords

Williams syndrome; diffusion tensor imaging; voxel-based analysis; tract-based analysis; fractional anisotropy; white matter

Please address correspondence to: Lori R. Arlinghaus, Ph.D., Vanderbilt University, Institute of Imaging Science, 1161 21st Avenue South, Medical Center North AA-1105, Nashville, TN 37232-2310, Phone: (615) 343-2022, Fax: (615) 322-0734, lori.arlinghaus@vanderbilt.edu.

1. Introduction

Williams syndrome (WS) is a disorder caused by a 1.5Mb hemizygous deletion on chromosome 7 (7q11.23) [1]. This deletion results in a unique set of physical, cognitive, and behavioral symptoms. Characteristic physical traits include unique cranio-facial features, such as a wide mouth with full lips and protrusive ears [2], and cardiovascular abnormalities [2, 3]. Individuals with WS typically exhibit mild to moderate mental retardation along with a unique combination of relative cognitive strengths and weaknesses, such as very good verbal short-term memory and poor visuospatial construction [4]. Behaviorally, individuals with WS typically demonstrate hypersociability and heightened empathy [5, 6], non-social anxiety [7], and sensitivity to loud or sudden noises [8, 9].

The diversity of symptoms exhibited in this syndrome suggests that multiple functional networks within the brain may be affected in different ways. This, along with evidence that several genes included in the typical WS deletion are involved in normal neural development and function [10–14], has led to increasing interest in studying the neural systems involved in the disorder. Magnetic resonance imaging (MRI) studies have revealed structural abnormalities, such as increased gyrification [15–17], reduced sulcal depth in the intraparietal and orbitofrontal sulci [18, 19], and a reduction in the extent of the central sulcus [20, 21]. Functional MRI (fMRI) studies have revealed differences in neural activation during tasks involving response inhibition [22], processing of fearful stimuli [23], visuospatial construction [24, 25], and auditory processing [26] in WS subjects compared to normal controls. Recently, diffusion tensor imaging (DTI) has been used to investigate white matter (WM) involvement in WS [27, 28], revealing multiple regions of both reduced and increased anisotropy throughout the brain.

These DTI studies used region of interest (ROI) analysis methods [27, 28] and tract-based spatial statistics (TBSS) [27]. In some cases, the differences in anisotropy found between the two groups were located within large WM bundles that contained multiple major WM tracts, making interpretation of the results more difficult than in WM regions consisting of a single tract. In the study described here, differences in fractional anisotropy (FA) were examined with a voxel-based comparison of young adults with WS and normal young adults to see if results from the previous studies could be replicated. A region of WM where multiple tracts merge was investigated further with a tract-based analysis, in an attempt to separate contributions from different WM tracts.

2. Methods

2.1. Subjects

Williams syndrome subjects were recruited from the annual music camp for young adults with Williams syndrome and other developmental disorders hosted by the Vanderbilt Kennedy Center for Research on Human Development, the Blair School of Music, and the National Williams Syndrome Association. Normal controls (NC) were recruited from the general population. Functional, structural, and diffusion tensor imaging scans were acquired for each subject during a single imaging session. Informed consent was obtained from each subject according to the requirements of the Institutional Review Board. DTI data sets from a total of 16 WS subjects and 16 NCs were compared. Structural images from an additional NC who did not have DTI data were used as the initial target for creation of a study-specific template used in the image co-registration process. The WS group consisted of 6 females and 10 males; all but 3 subjects were right handed; and their mean age was 24 years (range = 16 to 33 years). IQ scores for the WS group were assessed by the Kaufman Brief Intelligence Test (KBIT) [29]. The mean composite IQ for the group was 68 (range = 46 to 93 and standard deviation = 14) with a mean verbal score of 77 (range = 57 to 103 and

standard deviation = 12) and a mean nonverbal score of 56 (range = 20 to 94 and standard deviation = 23). The NC group consisted of 8 females and 8 males; 12 NCs were right-handed, 3 were left-handed and one was ambidextrous; and their mean age was 23 years (range = 16 to 32 years). IQ was not measured for the NC group. The target subject was a 19 year-old NC male who was right handed. A summary of the subject demographics is shown in Table 1. There was no significant difference in the mean age of the two groups (P = 0.255), and handedness was determined by the Edinburgh Handedness Inventory [30].

2.2. Image Acquisition

All images were acquired using a Philips Achieva 3T MRI scanner (Philips Healthcare, Best, The Netherlands) with high-performance gradient coils (80 mT/m gradient strength and 100 mT/m/ms slew-rate) and an 8 channel SENSE (sensitivity encoding) head coil. Diffusion weighted images (DWIs) were acquired with 32 diffusion-encoding directions (tr(b) = 1000 s/mm^2) and one non-diffusion-weighted image volume (tr(b) = 0 s/mm^2). Single-shot EPI and sensitivity encoding (SENSE) were used to decrease total scan time. The imaging parameters used were TE = 60 ms, TR = 10,000 ms, SENSE factor = 2, FOV = 256 × 256 mm^2, matrix size of 128 × 128, and 2 mm slice thickness. Whole-brain coverage was obtained with 60 axial slices in 6 minutes. A high-resolution, T1-weighted 3D anatomical volume was acquired using a multi-shot gradient echo sequence with TE = 4.6 ms, TR = 8.9 ms, SENSE factor = 2, FOV = 256 × 256 mm^2, and matrix size of 256 × 256. The volume consisted of 170 sagittal slices with an isotropic voxel size of 1 mm^3, and total scan time was 4 minutes and 24 seconds.

2.3. Image Processing

2.3.1. Tensor Calculation—Eddy current distortion and in-plane bulk subject motion were corrected within the original DWIs with the Philips Research Imaging Development Environment (PRIDE) Diffusion Registration tool (release 0.5). This tool performs an affine registration of each DWI to its corresponding non-diffusion-weighted image (b_0) [31]. The distortion- and motion-corrected DWIs were then used to calculate the diffusion tensor and FA maps, as well as extract the b_0 image volume, with a modified version of the PRIDE Fiber Tracking tool (Version 6.0a1). The in-house modifications to the tool included the addition of a routine to automatically reject from the tensor calculation data points corrupted by bulk and physiological motion. For each voxel, the residuals of the tensor fit are assumed to be normally distributed with a mean of zero, and data points with residuals greater than 3 standard deviations ($|z|$= 3) are considered to be outliers. However, the estimated mean and standard deviation (σ) of the residuals may be biased by outliers, so the value of (σ) must be calculated in a way that is robust to the effects of the outliers. The standard value (z) of each residual (r) is defined as

$$z=\frac{r-\mu}{\sigma}, \tag{1}$$

where μ is the mean of the residual values. By determining the value of the residuals that correspond to the 25th (r_{25}) and the 75th (r_{75}) percentiles, the value of (σ) can be solved for, since (μ) is assumed to be zero and the standard values for the 25th (z_{25}) and 75th (z_{75}) percentiles can be found in any standard normal table. The values of r_{25} and r_{75} are determined by

$$r_{25}=\text{MEDIAN}(r<0) \tag{2}$$

and

$$r_{75}=\text{MEDIAN}(r>0), \tag{3}$$

respectively, and $z_{25} = -0.6745$ and $z_{75} = 0.6745$ for a normal distribution. Substituting these values into Eq. 1 and solving for σ gives

$$\sigma=\frac{r_{75}-r_{25}}{1.349}. \tag{4}$$

2.3.2. Image Registration—Normalization of the FA maps was performed in two major steps. First, a study-specific FA template was created by normalizing each subject's FA map (FA_i, for the i^{th} subject) to the target T1-weighted image space ($T1_{targ}$) and then averaging the resulting images (FA_{temp}). Normalization of the FA maps was performed by combining the transformations from an intra-subject registration ($b_{0,i}$ to $T1_i$) and an inter-subject registration ($T1_i$ to $T1_{targ}$) to define the total transformation between the b=0 image space of each subject ($b_{0,i}$), which is inherently co-registered to FA_i, and the target T1-weighted image space ($T1_{targ}$). The resulting total transformation for each subject was then applied to FA_i, and the transformed FA maps were averaged to create the template (FA_{temp}). A diagram of the template creation process is shown in Fig. 1. Second, the original FA maps (FA_i) were co-registered directly to FA_{temp} to reduce potential bias introduced from the selection of a single normal control as the initial target.

All intermediate image registration steps were performed using linear [32, 33] and non-linear [34] registration software provided by the Medical Image Processing Laboratory in the Department of Electrical Engineering and Computer Science at Vanderbilt University. Intra-subject registration steps included a rigid registration to account for subject motion between the diffusion-weighted scan and the T1-weighted scan and then a nonlinear registration step to reduce the effects of image distortion. Inter-subject registration included a rigid registration with scaling to account for differences in head size and orientation between each subject and the target, as well as a nonlinear registration step to account for regional anatomical differences.

2.4. Voxel-based analysis—The normalized FA maps for the NC and WS groups were compared on a voxel-wise basis with a two-sample t-test. No smoothing was applied to the maps prior to analysis [35]. The resulting significance maps were thresholded at the $P < 0.05$ level. The significance maps were also masked so that only voxels with an average FA value of 0.3 or greater in the FA_{temp} remained to limit the analysis to the cores of the WM tracts, reducing the effects of minor registration errors. Permutation testing was performed with the same significance level and masking to determine the minimum significant cluster size (in 3 dimensions) according to the methods described by Bullmore et al. [36]. Only clusters with a volume greater than 90 voxels (90 mm^3) were considered to be significant ($P < 0.05$). The average FA template and map of significant clusters were transformed to the Talairach space for visualization.

2.5. Post hoc tract-based analysis—The left and right inferior fronto-occipital fasciculi and uncinate fasciculi were segmented, parameterized, and compared using a tract-based analysis. Briefly, a single voxel within the center of each end of the tract was defined in the common image space and then transformed to each subject's native image space. A large, spherical region of interest, centered about the transformed coordinates, was used to initiate multi-ROI fiber tracking to segment the tract-of-interest. The central axes of the resulting fiber tracts for each subject were then defined and parameterized in a way that also defined point correspondence across subjects [37–40]. Finally, FA values were compared

between groups at corresponding locations along each tract with a two-sample t-test and thresholded at a significance level of $P < 0.05$ (uncorrected).

3. Results

On visual inspection, image normalization appeared to perform well in the larger WM structures, with reliability decreasing for smaller WM tracts and for tracts branching off to cortical areas, particularly in the parietal and occipital lobes. This was confirmed quantitatively by calculating (separately) the within-group variance of the normalized FA maps for both the CO and WS groups.

3.1. Voxel-based analysis

Significant differences in FA between the two groups were found in several regions where image normalization performed well. Fig. 2 shows the overlay of the significance map on the average FA template. The mean FA of the WS subjects compared to NCs was decreased in the splenium of the corpus callosum, bilateral corona radiata, external capsules (EC), cortico-spinal/cortico-cerebellar tracts extending from the pons through the posterior limb of the external capsules (PLIC), uncinate fasciculi (UF)/inferior front-occipital fasciculus (IFO), and superior longitudinal fasciculi (SLF). An increase in mean FA in WS was found in the left IFO/inferior longitudinal fasciculus (ILF), bilateral SLF (right > left), and bilateral UF. (See Table 2 for a list of representative Talairach coordinates for these regions.) Note that a given anatomical structure can have positive and negative changes at different positions along the tract. Significant clusters were also found in regions where image normalization performed poorly: bilateral forceps major, anterior commissure, prefrontal WM, ventral cingulum, fornix, cerebellar peduncles, and WM underlying the intraparietal sulci; these regions were discarded from further analysis.

3.2. Tract-based analysis

The right and left uncinate and the left inferior fronto-occipital tracts were successfully tracked in each subject. The right inferior fronto-occipital tract was successfully tracked in all NCs and all but 2 WS subjects, where only a single fiber was found in this tract. Fig. 3 shows the plots of the mean FA values for each group as a function of position along the tracts, as well as a display of the mean axes for each subject (in the common image space) with regions of significant differences highlighted. The left uncinate contained two large regions of increased FA (WS > NC) and a small region of decreased FA (WS < NC) in the portion passing through the EC in the WS group compared to NCs. An additional small region of reduced FA was also found in the temporal portion of the tract. The right uncinate contained a region of reduced FA at the anterior extent of the portion passing through the EC, as well as a small region of reduced FA in the portion of the tract extending into frontal WM. The left IFO contained a single region of reduced FA in the portion passing through the EC, as well as an additional region of reduced FA in the temporal portion of the tract and two regions of increased FA in the occipital portion of the tract. The right IFO contained a large region of increased FA in the portion passing through the EC, as well as an additional region of increased FA in the temporal portion of the tract.

4. Discussion

We performed a voxel-based comparison of FA between young adults with Williams syndrome and normal controls and found several regions of WM with increased FA, as well as several regions with decreased FA, in the WS subjects. These results are generally consistent with previously reported differences in WM diffusion parameters between subjects with WS and normal controls [27, 28].

Decreased FA in the splenium of the corpus callosum is consistent with the findings of Hoeft et al. [27], as well as reports of altered shape and reduced volume in the posterior portion of the corpus callosum in WS [41–43]. Changes in this posterior portion of the corpus callosum, which contains fibers connecting the right and left parietal and occipital lobes, may be related to the visuospatial deficits associated with the disorder [41].

Another major WM tract with changes in FA that is potentially involved in visuospatial deficits is the SLF, which contains connections between the frontal, parietal, and temporal lobes. Hoeft et al. reported increased FA in both the right and left SLF (right > left) and a negative correlation of FA in the right SLF with scores from the WAIS-III Object Assembly subtest [27]. We also found regions of increased FA in both the left and right parietal portion of the SLF, with larger cluster size in the right SLF. Unlike Hoeft et al., however, we also found small regions of reduced FA in projections to the precentral gyri from both the left and right SLF. These regions of reduced FA were near the lateral premotor cortex (Brodmann area 6), which has connections to the parietal lobe (Brodmann area 40) through the SLF [44, 45], and it has been shown that they are important for movement that relies on external cues [46].

Our finding of decreased FA in the bilateral PLIC is consistent with the Hoeft [27] and Marenco [28] studies, which also reported bilateral reductions of anisotropy in these regions, and the extent of the regions of reduced FA we observed was quite remarkable. (See Fig. 2, $Z=-12$ to $Z=-20$.) Both regions extended from the level of the pons to the level of the superior portion of the thalamus and include several WM pathways important in motor and sensory function, such as the corticobulbar (cranial motor function), corticospinal (motor function in the body), corticorubral (motor coordination), thalamocortical (sensory and motor function), and corticopontine (relay between motor cortex and cerebellum) tracts. While mild motor symptoms have been noted in the literature [47, 48], it has not been until recently that quantitative studies of motor signs and symptoms in WS have been published. Gagliardi et al. [49] reported the existence of cerebellar, pyramidal, and extrapyramidal signs that varied in distribution according to age. Hocking et al. [50] studied abnormal gait characteristics in adults with WS and suggested that basal ganglia dysfunction and visuomotor deficits may be involved. Quantitative measures of neurological signs or symptoms in the WS cohort in this study were not obtained; however, research staff were able to provide evaluations of gross motor deficits, confirming the existence of abnormal gait and muscle weakness in several of the WS subjects in this study (data not shown).

Results in the WM regions containing the ILF and IFO vary between this study and the studies published by Hoeft et al. [27] and Marenco et al. [28]. We found increased FA in the left ILF/IFO only, while Hoeft et al. reported significantly increased FA in the right ILF only, and Marenco et al. found increased anisotropy in tract-based ROIs averaged over both hemispheres. This region of WM contains fiber pathways associated with face and object recognition, and it has been proposed that while face processing abilities seem to be relatively intact in WS, higher-level object recognition and face processing may actually be functioning abnormally [51, 52]. Perhaps also related to the ILF, Thornton-Wells et al. (2010) reported evidence of cross-modal sensory processing (activation of the visual cortex during auditory perception) that might be supported by increased connectivity of the temporal and occipital lobes [26].

We found that the bilateral EC also contained regions of both increased and decreased FA, while Hoeft et al. reported only increased FA. An additional region of WM in the UF/IFO, slightly anterior to the EC, showed reduced FA bilaterally. Changes in the EC and frontal WM might be related to the social aspects of the disorder. The UF and IFO, two major association pathways with connections to the frontal lobes, pass through this region, as well

as several smaller tracts, which include connections between the frontal lobe and the basal ganglia and amygdala. The UF also contains connections between the amygdala and temporal lobe structures [53]. Functional connections between the cortical regions connected by pathways passing through the EC have been shown to be disrupted in WS. Mobbs et al. [22] reported abnormal activity in the striatum, dorsolateral prefrontal, and dorsal cingulate cortices in an fMRI study of response inhibition. Also,an fMRI study designed to invoke activation in the amygdala from threatening visual stimuli by Meyer-Lindenberg et al. [23] suggested that functional connections between different regions of frontal cortices and the amygdala may be disrupted.

It is difficult to interpret the underlying cause of the differences in FA between the WS and NC groups observed in this study because the diffusion tensor is sensitive to changes in local tissue microstructure, such as cell density, edema, and demyelination, as well as differences in structural organization. Marenco et al. [28] hypothesized that changes they found in the principal orientation of WM tissue in several association tracts indicated that WM fibers that normally developed in the right-left orientation either changed course during development or failed to develop. However, as Hoeft et al. [27] pointed out, it is also possible that the orientational differences Marenco et al. observed and the increases in FA observed in this study and the study by Hoeft et al. indicates a decrease in normal branching of these tracts to cortical regions along their paths. Decreased branching might lead to a decrease in the normal amount of fiber crossing, resulting in an increase in FA. This hypothesis is consistent with evidence that the LIMK1 and CYLN2 genes included in the typical WS deletion are involved in normal neuronal migration and development [13, 54, 55]. LIMK1 is required for proper functioning of an axonal guidance protein called semaphorin 3A in neural migration [54]. This same protein has also been shown to be involved in normal pruning of axonal branches in hippocampal neurons [56]. Furthermore, neurotrophin nerve growth factor (NGF), which is crucial for terminal arborization and neuronal survival, is elevated during typical development from 2 to 6 years of age but has been shown to be elevated more than four times as long in persons with WS, from 2 to 20 years of age, which could interfere with normal axonal pruning [57, 58]. In early development, axons send out many branches to different functional areas, which are selectively pruned later in development as the brain refines itself. Perhaps, while some regions experience a decrease in branching causing an increase in FA, other regions may initially develop normal branching that is never properly pruned, causing a decrease in FA.

An additional consideration that should be made in the interpretation of the results reported here is the fact that there were methodological differences between this study and the studies by Hoeft et al. and Marenco et al. Both of the previous studies had 10 or fewer subjects per group and acquired multiple sets of 6 diffusion directions. We compared 16 WS subjects with 16 controls and acquired a single set of 32 diffusion directions, which has been shown to provide a better estimation of anisotropy than multiple acquisitions of fewer than 20 directions [59]. We performed a voxel-based comparison, which allowed us to explore the entire brain for changes without restriction to a priori knowledge of regions or tracts of interest. However, a major limitation of this analysis technique is that it relies upon accurate image co-registration. While the registration algorithms we used are sophisticated and great care was taken to ensure the best possible co-registration, anatomical variability between subjects makes it impossible for the algorithms to produce a perfect result. Registration results are generally best in large WM structures near the center of the brain, such as the internal capsule and corpus callosum, and the quality decreases as the structures get smaller in size and closer to the cortex, where differences in gyrification can be particularly problematic.

Even within well-registered large WM structures, the registration algorithms typically used have no way of determining whether smaller WM tracts within the larger structure are properly aligned across subjects. This creates ambiguity in regions of WM that contain multiple WM tracts. An example from this study is the external capsule. There is no way of knowing whether changes in the uncinate fasciculi, inferior fronto-occipital fasciculi, or both are the cause of the significant differences in FA that we observed. Hoeft et al. faced a similar dilemma in their findings in the inferior longitudinal fasciculus (ILF) in both an ROI-style and a tract-base spatial statistics (TBSS) analysis [60], where neither method could distinguish between the ILF and IFO. Marenco et al. averaged diffusion parameters over pairs of entire WM tracts segmented by fiber tractography, which reduces sensitivity to localized changes, particularly since diffusion parameters can vary greatly along fiber tracts.

In an attempt to overcome these challenges, we further examined the major white matter tracts passing through the EC with a tract-based analysis. We compared FA values between a group of young adults with WS and a group of normal controls along the uncinate and inferior fronto-occipital fasciculi, the two major WM pathways that pass through the inferior portion of the external capsules, and found regions of significantly different FA in all four tracts. Our results were consistent with the findings from the voxel-based analysis and the two previously published studies of WS with DTI [27, 28]. The results from the voxel-based comparison of these data suggested that the FA differences in the EC were fairly similar between hemispheres. However, the results of this tract-specific comparison indicate that the left and right uncinate fasciculi and IFO each contribute to changes in FA in the EC in different ways. This is not entirely surprising, given that there is evidence of functional lateralization associated with these WM tracts. The uncinate fasciculi connect regions in the frontal (mainly orbitofrontal) lobes with regions in the temporal lobes, including the amygdala [61, 62]. There is evidence of lateralization in the function of the amygdala [63], and an fMRI study of WS designed to invoke activation in the amygdala from threatening visual stimuli by Meyer-Lindenberg et al. [23] revealed reduced activation in the amygdalae of WS subjects compared to normal controls, with the difference much more pronounced in the right hemisphere. Further investigation of the functional network involved in this observed dysfunction suggested that normal functional connections between different regions of frontal cortices and the amygdala may be disrupted. While the path analyses implemented by Meyer-Lindenberg et al. are not meant to be interpreted as direct connections between anatomical locations, it is certainly possible that the reduced FA observed in the right uncinate is involved. As discussed above, the IFO tracts might underlie behavioral differences in face processing and language tasks, as well.

In conclusion, the evidence from this study and previous DTI studies of WS is consistent with structural, functional, and behavioral differences found in the disorder and warrant further study to improve our understanding of the role of white matter changes. The tract-based analysis method used in the paper allowed us to demonstrate its usefulness in the investigation of the role of specific white matter tracts in behavioral and cognitive dysfunction in Williams syndrome. To the best of our knowledge, it is the first of its kind in the study of Williams syndrome. Previous DTI studies that included fiber tracking could not identify localized changes within the tracts or assign involvement to particular tracts in regions of WM where multiple fiber pathways traveled together. Hopefully, more precise knowledge of the specific WM tracts affected in WS will aid in the design of future functional, structural, and behavioral studies of the disorder.

Acknowledgments

We would like to thank Dr. Benoit Dawant for providing the registration software. This work was supported by the National Institutes of Health grant NIH RO1 EB00277.

References

1. Peoples R, Franke Y, Wang YK, Pérez-Jurado L, Paperna T, Cisco M, Francke U. A physical map, including a BAC/PAC clone contig, of the Williams-Beuren syndrome-deletion region at 7q11.23. Am J Hum Genet. 2000; 66(1):47–68. [PubMed: 10631136]
2. Beuren AJ, Apitz J, Harmjanz D. Supravalvular aortic stenosis in association with mental retardation and a certain facial appearance. Circulation. 1962; 26:1235–1240. [PubMed: 13967885]
3. Williams JC, Barratt-Boyes BG, Lowe JB. Supravalvular aortic stenosis. Circulation. 1961; 24:1311–1318. [PubMed: 14007182]
4. Mervis CB, Robinson BF, Bertrand J, Morris CA, Klein-Tasman BP, Armstrong SC. The Williams syndrome cognitive profile. Brain Cogn. 2000; 44(3):604–628. [PubMed: 11104544]
5. Bellugi U, Adolphs R, Cassady C, Chiles M. Towards the neural basis for hypersociability in a genetic syndrome. Neuroreport. 1999; 10(8):1653–1657. [PubMed: 10501552]
6. Klein-Tasman BP, Mervis CB. Distinctive personality characteristics of 8-, 9-, and 10-year-olds with Williams syndrome. Dev Neuropsych. 2003; 23(1–2):269–290.
7. Dykens EM. Anxiety, fears, phobias in persons with Williams syndrome. Dev Neuropsychol. 2003; 23(1–2):291–316. [PubMed: 12730029]
8. Klein AJ, Armstrong BL, Greer MK, Brown FR. Hyperacusis and otitis media in individuals with Williams syndrome. J Speech Hear Disord. 1990; 55(2):339–344. [PubMed: 2329796]
9. Levitin DJ, Cole K, Lincoln A, Bellugi U. Aversion, awareness, attraction: investigating claims of hyperacusis in the Williams syndrome phenotype. J Child Psychol Psychiatry. 2005; 46(5):514–523. [PubMed: 15845131]
10. Hoogenraad CC, Koekkoek B, Akhmanova A, Krugers H, Dortland B, Miedema M, van Alphen A, Kistler WM, Jaegle M, Koutsourakis M, Camp NV, Verhoye M, van der Linden A, Kaverina I, Grosveld F, Zeeuw CID, Galjart N. Targeted mutation of Cyln2 in the Williams syndrome critical region links CLIP-115 haploinsufficiency to neurodevelopmental abnormalities in mice. Nat Genet. 2002; 32(1):116–127. [PubMed: 12195424]
11. Igaz, LMl; Bekinschtein, P.; Izquierdo, In; Medina, JH. One-trial aversive learning induces late changes in hippocampal CaMKII[alpha], Homer 1a, Syntaxin 1a and ERK2 protein levels. Mol Brain Res. 2004; 132(1):1–12. [PubMed: 15548423]
12. Meng Y, Zhang Y, Tregoubov V, Janus C, Cruz L, Jackson M, Lu WY, MacDonald JF, Wang JY, Falls DL, Jia Z. Abnormal spine morphology and enhanced LTP in LIMK-1 knockout mice. Neuron. 2002; 35(1):121–133. [PubMed: 12123613]
13. De Zeeuw CI, Hoogenraad CC, Goedknegt E, Hertzberg E, Neubauer A, Grosveld F, Galjart N. CLIP-115, a novel brain-specific cytoplasmic linker protein, mediates the localization of dendritic lamellar bodies. Neuron. 1997; 19(6):1187–1199. [PubMed: 9427243]
14. Zhao C, Aviles C, Abel RA, Almli CR, McQuillen P, Pleasure SJ. Hippocampal and visuospatial learning defects in mice with a deletion of frizzled 9, a gene in the Williams syndrome deletion interval. Development. 2005; 132(12):2917–2927. [PubMed: 15930120]
15. Schmitt JE, Watts K, Eliez S, Bellugi U, Galaburda AM, Reiss AL. Increased gyrification in Williams syndrome: evidence using 3D MRI methods. Dev Med Child Neurol. 2002; 44(5):292–295. [PubMed: 12033713]
16. Thompson PM, Lee AD, Dutton RA, Geaga JA, Hayashi KM, Eckert MA, Bellugi U, Galaburda AM, Korenberg JR, Mills DL, Toga AW, Reiss AL. Abnormal cortical complexity and thickness profiles mapped in Williams syndrome. J Neurosci. 2005; 25(16):4146–4158. [PubMed: 15843618]
17. Gaser C, Luders E, Thompson PM, Lee AD, Dutton RA, Geaga JA, Hayashi KM, Bellugi U, Galaburda AM, Korenberg JR, Mills DL, Toga AW, Reiss AL. Increased local gyrification mapped in Williams syndrome. NeuroImage. 2006; 33(1):46–54. [PubMed: 16901723]
18. Kippenhan JS, Olsen RK, Mervis CB, Morris CA, Kohn P, Meyer-Lindenberg A, Berman KF. Genetic contributions to human gyrification: sulcal morphometry in Williams syndrome. J Neurosci. 2005; 25(34):7840–7846. [PubMed: 16120786]

19. Van Essen DC, Dierker D, Snyder AZ, Raichle ME, Reiss AL, Korenberg J. Symmetry of cortical folding abnormalities in Williams syndrome revealed by surface-based analyses. J Neurosci. 2006; 26(20):5470–5483. [PubMed: 16707799]
20. Galaburda AM, Schmitt JE, Atlas SW, Eliez S, Bellugi U, Reiss AL. Dorsal forebrain anomaly in Williams syndrome. Arch Neurol. 2001; 58(11):1865–1869. [PubMed: 11708996]
21. Jackowski AP, Schultz RT. Foreshortened dorsal extension of the central sulcus in Williams syndrome. Cortex. 2005; 41(3):282–290. [PubMed: 15871594]
22. Mobbs D, Eckert MA, Mills D, Korenberg J, Bellugi U, Galaburda AM, Reiss AL. Frontostriatal dysfunction during response inhibition in Williams syndrome. Biol Psychiatry. 2007; 62(3):256–261. [PubMed: 16996488]
23. Meyer-Lindenberg A, Hariri AR, Munoz KE, Mervis CB, Mattay VS, Morris CA, Berman KF. Neural correlates of genetically abnormal social cognition in Williams syndrome. Nat Neurosci. 2005; 8(8):991–993. [PubMed: 16007084]
24. Meyer-Lindenberg A, Kohn P, Mervis CB, Kippenhan JS, Olsen RK, Morris CA, Berman KF. Neural basis of genetically determined visuospatial construction deficit in Williams syndrome. Neuron. 2004; 43(5):623–631. [PubMed: 15339645]
25. Meyer-Lindenberg A, Mervis CB, Sarpal D, Koch P, Steele S, Kohn P, Marenco S, Morris CA, Das S, Kippenhan S, Mattay VS, Weinberger DR, Berman KF. Functional, structural, metabolic abnormalities of the hippocampal formation in Williams syndrome. J Clin Invest. 2005; 115(7): 1888–1895. [PubMed: 15951840]
26. Thornton-Wells TA, Cannistraci CJ, Anderson AW, Kim CY, Eapen M, Gore JC, Blake R, Dykens EM. Auditory Attraction: Activation of Visual Cortex by Music and Sound in Williams Syndrome. Am J Intellect Dev Disabil. 2010; 115(2):172–189. [PubMed: 20440382]
27. Hoeft F, Barnea-Goraly N, Haas BW, Golarai G, Ng D, Mills D, Korenberg J, Bellugi U, Galaburda A, Reiss AL. More is not always better: increased fractional anisotropy of superior longitudinal fasciculus associated with poor visuospatial abilities in Williams syndrome. J Neurosci. 2007; 27(44):11960–11965. [PubMed: 17978036]
28. Marenco S, Siuta MA, Kippenhan JS, Grodofsky S, Chang W-L, Kohn P, Mervis CB, Morris CA, Weinberger DR, Meyer-Lindenberg A, Pierpaoli C, Berman KF. Genetic contributions to white matter architecture revealed by diffusion tensor imaging in Williams syndrome. Proc Natl Acad Sci U S A. 2007; 104(38):15117–15122. [PubMed: 17827280]
29. Kaufman, AS.; Kaufman, NL. Kaufman Brief Intelligence Test manual. Circle Pines, MN: American Guidance Service; 1990.
30. Oldfield RC. The assessment and analysis of handedness: the Edinburgh inventory. Neuropsychologia. 1971; 9(1):97–113. [PubMed: 5146491]
31. Netsch T, van Muiswinkel A. Quantitative evaluation of image-based distortion correction in diffusion tensor imaging. IEEE Trans Med Imaging. 2004; 23(7):789–798. [PubMed: 15250631]
32. Maes F, Collignon A, Vandermeulen D, Marchal G, Suetens P. Multimodality image registration by maximization of mutual information. IEEE Trans Med Imaging. 1997; 16(2):187–198. [PubMed: 9101328]
33. Li, R. Automatic placement of regions of interest in medical images using image registration. Vanderbilt University; 2001.
34. Rohde GK, Aldroubi A, Dawant BM. The adaptive bases algorithm for intensity-based nonrigid image registration. IEEE Trans Med Imaging. 2003; 22(11):1470–1479. [PubMed: 14606680]
35. Jones DK, Symms MR, Cercignani M, Howard RJ. The effect of filter size on VBM analyses of DT-MRI data. Neuroimage. 2005; 26(2):546–554. [PubMed: 15907311]
36. Bullmore ET, Suckling J, Overmeyer S, Rabe-Hesketh S, Taylor E, Brammer MJ. Global, voxel, cluster tests, by theory and permutation, for a difference between two groups of structural MR images of the brain. IEEE Trans Med Imaging. 1999; 18(1):32–42. [PubMed: 10193695]
37. Corouge I, Fletcher PT, Joshi S, Gouttard S, Gerig G. Fiber tract-oriented statistics for quantitative diffusion tensor MRI analysis. Med Image Anal. 2006; 10(5):786–798. [PubMed: 16926104]
38. Corouge I, Gouttard S, Gerig G. Towards a shape model of white matter fiber bundles using diffusion tensor MRI. IEEE International Symposium on Biomedical Imaging: Nano to Macro. 2004:344–347.

39. Ding Z, Gore JC, Anderson AW. Classification and quantification of neuronal fiber pathways using diffusion tensor MRI. Magn Reson Med. 2003; 49(4):716–721. [PubMed: 12652543]
40. Zhang S, Correia S, Laidlaw DH. Identifying White-Matter Fiber Bundles in DTI Data Using an Automated Proximity-Based Fiber-Clustering Method. IEEE Trans Vis Comput Graph. 2008; 14(5):1044–1053. [PubMed: 18599916]
41. Schmitt JE, Eliez S, Warsofsky IS, Bellugi U, Reiss AL. Corpus callosum morphology of Williams syndrome: relation to genetics and behavior. Dev Med Child Neurol. 2001; 43(3):155–159. [PubMed: 11263684]
42. Tomaiuolo F, Paola MD, Caravale B, Vicari S, Petrides M, Caltagirone C. Morphology and morphometry of the corpus callosum in Williams syndrome: a T1-weighted MRI study. Neuroreport. 2002; 13(17):2281–2284. [PubMed: 12488811]
43. Luders E, Paola MD, Tomaiuolo F, Thompson PM, Toga AW, Vicari S, Petrides M, Caltagirone C. Callosal morphology in Williams syndrome: a new evaluation of shape and thickness. Neuroreport. 2007; 18(3):203–207. [PubMed: 17314657]
44. Cipolloni PB, Pandya DN. Cortical connections of the frontoparietal opercular areas in the rhesus monkey. J Comp Neurol. 1999; 403(4):431–458. [PubMed: 9888311]
45. Petrides M, Pandya DN. Projections to the Frontal-Cortex from the Posterior Parietal Region in the Rhesus-Monkey. J Comp Neurol. 1984; 228(1):105–116. [PubMed: 6480903]
46. Kuruma H, Watanabe S, Ikeda Y, Senoo A, Kikuchi Y, Abo M, Yonemoto K. Neural mechanism of self-initiated and externally triggered finger movements. Journal of Physical Therapy Science. 2007; 19(2):103–109.
47. Trauner DA, Bellugi U, Chase C. Neurologic features of Williams and Down syndromes. Pediatr Neurol. 1989; 5(3):166–168. [PubMed: 2525908]
48. Chapman CA, du Plessis A, Pober BR. Neurologic findings in children and adults with Williams syndrome. J Child Neurol. 1996; 11(1):63–65. [PubMed: 8745391]
49. Gagliardi C, Martelli S, Burt MD, Borgatti R. Evolution of neurologic features in Williams syndrome. Pediatr Neurol. 2007; 36(5):301–306. [PubMed: 17509461]
50. Hocking DR, Rinehart NJ, McGinley JL, Bradshaw JL. Gait function in adults with Williams syndrome. Exp Brain Res. 2009; 192(4):695–702. [PubMed: 18841354]
51. Mobbs D, Garrett AS, Menon V, Rose FE, Bellugi U, Reiss AL. Anomalous brain activation during face and gaze processing in Williams syndrome. Neurology. 2004; 62(11):2070–2076. [PubMed: 15184616]
52. Sarpal D, Buchsbaum BR, Kohn PD, Kippenhan JS, Mervis CB, Morris CA, Meyer-Lindenberg A, Berman KF. A genetic model for understanding higher order visual processing: functional interactions of the ventral visual stream in williams syndrome. Cereb Cortex. 2008; 18(10):2402–2409. [PubMed: 18308711]
53. Klingler J, Gloor P. The connections of the amygdala and of the anterior temporal cortex in the human brain. J Comp Neurol. 1960; 115:333–369. [PubMed: 13756891]
54. Aizawa H, Wakatsuki S, Ishii A, Moriyama K, Sasaki Y, Ohashi K, Sekine-Aizawa Y, Sehara-Fujisawa A, Mizuno K, Goshima Y, Yahara I. Phosphorylation of cofilin by LIM-kinase is necessary for semaphorin 3A-induced growth cone collapse. Nat Neurosci. 2001; 4(4):367–373. [PubMed: 11276226]
55. Endo M, Ohashi K, Sasaki Y, Goshima Y, Niwa R, Uemura T, Mizuno K. Control of Growth Cone Motility and Morphology by LIM Kinase and Slingshot via Phosphorylation and Dephosphorylation of Cofilin. J Neurosci. 2003; 23(7):2527–2537. [PubMed: 12684437]
56. Bagri A, Cheng H, Yaron A, Pleasure SJ, Tessier-Lavigne M. Stereotyped Pruning of Long Hippocampal Axon Branches Triggered by Retraction Inducers of the Semaphorin Family. Cell. 2003; 113(3):285–299. [PubMed: 12732138]
57. Calamandrei G, Alleva E, Cirulli F, Queyras A, Volterra V, Capirci O, Vicari S, Giannotti A, Turrini P, Aloe L. Serum NGF levels in children and adolescents with either Williams syndrome or Down syndrome. Dev Med Child Neurol. 2000; 42(11):746–750. [PubMed: 11104346]
58. Deppmann CD, Mihalas S, Sharma N, Lonze BE, Niebur E, Ginty DD. A model for neuronal competition during development. Science. 2008; 320(5874):369–373. [PubMed: 18323418]

59. Jones DK. The effect of gradient sampling schemes on measures derived from diffusion tensor MRI: a Monte Carlo study. Magn Reson Med. 2004; 51(4):807–815. [PubMed: 15065255]

60. Smith SM, Jenkinson M, Johansen-Berg H, Rueckert D, Nichols TE, Mackay CE, Watkins KE, Ciccarelli O, Cader MZ, Matthews PM, Behrens TE. Tract-based spatial statistics: voxelwise analysis of multi-subject diffusion data. Neuroimage. 2006; 31(4):1487–1505. [PubMed: 16624579]

61. Ebeling U, von Cramon D. Topography of the uncinate fascicle and adjacent temporal fiber tracts. Acta Neurochir (Wien). 1992; 115(3–4):143–148. [PubMed: 1605083]

62. Moran MA, Mufson EJ, Mesulam M. Neural inputs into the temporopolar cortex of the rhesus monkey. J Comp Neurol. 1987; 256(1):88–103. [PubMed: 3819040]

63. Baas D, Aleman A, Kahn RS. Lateralization of amygdala activation: a systematic review of functional neuroimaging studies. Brain Res Rev. 2004; 45(2):96–103. [PubMed: 15145620]

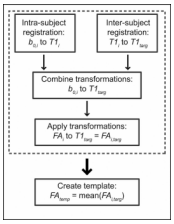

Figure 1.
Schematic of the process used to create the study-specific FA template (FA_{temp}) used for image normalization. First, each subject's FA map was transformed to the T1targ image space (dashed box), then the average of all the subjects' transformed FA maps was calculated and used as the FA template for the second step of the registration process.

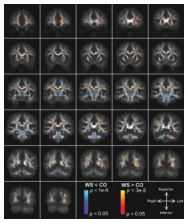

Figure 2.
Voxel-based comparison of FA in WS compared to NC. Overlay of regions of significantly increased (warm colors) and reduced (cool colors) FA in WS compared to controls on coronal slices of the average FA template in Talairach space. (Images displayed according to radiological convention. i.e., the left hemisphere is shown on the right.)

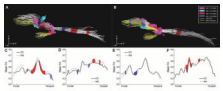

Figure 3.
Tract-based comparison of FA of two major WM tracts in the external capsule in WS compared to NC. The mean axes of the left (A) and right (B) uncinate (yellow) and inferior fronto-occipital (white) fasciculi from each subject are displayed together as viewed from the left. Regions of significantly ($P < 0.05$) reduced and increased FA are marked in blue and red, respectively. Regions of significantly increased (magenta) and decreased (cyan) FA found near the EC in the voxel-based analysis are also shown for comparison, and orientation is marked as follows: anterior (A), left (L), superior (S), and inferior (I). Mean FA values for each group are plotted as a function of position along the left uncinate (C), left inferior fronto-occipital tract (D), right uncinate (E), and right inferior fronto-occipital tract (F), with regions of significantly reduced and increased FA marked in blue and red, respectively.

Table 1

Subject demographics

Group		N	Age (years)			Handedness		
			Range	Mean	Standard deviation	Right	Left	Ambidextrous
Controls	Male	8	18 – 32	23	5	5	2	1
	Female	8	16 – 26	22	3.5	7	1	0
	Total	16	16 – 32	23	4	12	3	1
Williams	Male	10	16 – 33	24	5	7	3	0
syndrome	Female	6	16 – 30	24	5	6	0	0
	Total	16	16 – 33	24	5.5	13	3	0

Table 2

Voxel-based analysis results

WM Region	Talairach Coordinates		
	X	Y	Z
Decreased FA			
Corona radiata (L)	−15	−6	45
Corona radiata (R)	17	−6	44
External capsule (L)	−26	9	8
External capsule (R)	27	9	8
PLIC (L)	−20	−18	5
PLIC (R)	21	−18	5
Splenium	1	−36	12
SLF (L)	−39	−11	31
SLF (R)	41	−8	28
Uncinate/IFO (L)	−17	19	−9
Uncinate/IFO (R)	17	19	−9
Increased FA			
External capsule (L)	−29	5	−5
External capsule (R)	27	8	−3
ILF/IFO (L)	−38	−37	−4
SLF (L)	−42	−30	26
SLF (R)	37	−25	32
SLF (L)	−37	−44	21
SLF (R)	33	−42	21